Performance Analysis of Decentralized Kalman Filters under Communication Constraints

MARKUS S. SCHLOSSER
KRISTIAN KROSCHEL

Distributed fusion architectures are often used in multi-sensor target tracking as they are more robust and more flexible than centralized architectures. Furthermore, they allow for a reduction in the required communication bandwidth with only limited effect on the estimation performance. The trade-off between bandwidth and performance is analyzed in detail for the special case of a decentralized Kalman filter. As a result of this study, a conservative fusion approach for such systems with a reduced communication rate is proposed.

Manuscript received August 20, 2004; revised April 13, 2006, November 4, 2006, and October 8, 2007; released for publication November 8, 2007.

Refereeing of this contribution was handled by Benjamin Slocumb.

This work is part of the Sonderforschungsbereich (SFB) No. 588 *"Humanoide Roboter—Lernende und kooperierende multimodale Roboter"* at the University of Karlsruhe. The SFB is supported by the Deutsche Forschungsgemeinschaft (DFG).

Authors' addresses: M. S. Schlosser, Deutsche Thomson OHG, Karl-Wiechert-Allee 74, 30625 Hannover, Germany, E-mail: (markus.schlosser@thomson.net); K. Kroschel, Institut für Nachrichtentechnik, Universität Karlsruhe, 76128 Karlsruhe, Germany, E-mail: (kroschel@int.uni-karlsruhe.de).

1. INTRODUCTION

In target tracking, multi-sensor systems are becoming more and more popular [14]. The advantages especially for physically distributed sensors are obvious: multiple viewing angles, different strong points of different sensors, and a higher robustness due to the inherent redundancy. On the other hand, some kind of fusion is necessary to integrate the data from the different sensors and to extract the desired information about the targets.

Traditionally, centralized fusion architectures have been used as their application is straightforward. All the data from the different sensors is sent to a single location to be fused. In recent years, increasing emphasis has been placed on distributed fusion where several fusion nodes exist in the network, like e.g., the Decentralized Kalman Filter (DKF) [11, 27], which is studied here, but also the covariance method [2], the federated filter [6, 7], a fusion system based on channel filters [23], and, most recently, a unified framework for optimal linear estimation fusion [16–21, 29].

As usual, the approaches based on Kalman filters are thereby mainly restricted to the linear Gaussian case. Furthermore, the unified framework is theoretically very insightful. As detailed in [17], the required generalized covariance matrix can, however, only be calculated accurately for some special cases. In many cases, it needs to be approximated numerically or even manually tuned. Finally, even if the covariance matrix can be determined accurately, this need not necessarily be possible in a recursive way so that no recursive estimator can be designed [16].

In a distributed fusion system, the sensor measurements are processed locally to produce state estimates, which are then transmitted between the fusion nodes. This approach is conceptually more complex as, even for statistically independent measurements, the local state estimates are correlated in time and among each other. In contrast to centralized fusion, there is also the danger of reusing information. Common information has to be detected and discarded in the fusion process. Additionally, the task of data association in tracking multiple targets, which is already difficult and still an active area of research for centralized architectures [4], becomes even more complex in the distributed case where only parts of the data are available at each fusion node. Finally, distributed fusion can even be inherently suboptimal [18]. A sufficient condition for distributed fusion to be optimal, however, is that the measurement noises are uncorrelated, which is often at least approximately given in real world scenarios.

On the other hand, the advantages of such distributed fusion architectures are a higher robustness due to a redundancy of fusion nodes and a lower processing load at each fusion node. It is also easier to integrate or scale existing systems. Therefore, distributed fusion is espe-

cially advantageous for large scale systems with many sensors. For such a system, another problem typically consists in only a limited amount of communication bandwidth being available. In this case, distributed fusion opens up the possibility to trade off bandwidth against performance by letting the fusion nodes communicate at reduced rates.

In [8, 12, 22], it was already pointed out that, if the communication rate is reduced, the information conveyed by the different local processors becomes correlated due to propagating the same underlying process noise. However, no quantitative measures for the amount of performance degradation were given. In [10], formulas describing the steady state performance of a DKF for arbitrary communication rates were derived and compared with simulative results for a linear system with two sensors and a nearly constant velocity model for the target dynamics. In our work, a simple formula for the performance degradation in the worst case of ignoring the correlation completely is derived. Its evaluation is straightforward compared with the solution of the asymmetric Lyapunov equation in [10]. As it represents the worst case, this analysis can be used to turn the too optimistic estimates of a system with reduced communication rate into conservative ones. Furthermore, the simulative study is extended to a nearly constant acceleration model, which results in some further insights.

The rest of this paper is organized as follows: The Decentralized Kalman Filter (DKF) is introduced in Section 2. In Section 3, the bandwidth requirements of centralized and distributed fusion architectures are compared with each other. The possibility for a reduction in communication rate is detailed in Section 4, and the resulting performance analyzed in Section 5. Based on the results, a new conservative fusion approach is proposed in Section 6. Finally, Section 7 recapitulates the most important findings.

2. DECENTRALIZED KALMAN FILTER

For a Kalman Filter (KF) to be applicable, the target's dynamics need to be modeled by the following state space equation

$$\mathbf{x}(k+1) = \mathbf{F}\mathbf{x}(k) + \mathbf{w}(k) \tag{1}$$

where $\mathbf{x}(k)$ is the state vector of the target at time instant k, typically containing the target position, velocity etc. $\mathbf{F}$ is the time-invariant state transition matrix and $\mathbf{w}(k)$ a white noise sequence with covariance matrix $\mathbf{Q}(k)$ representing the process noise. The state transition matrix $\mathbf{F}$ could just as well be time-variant for a KF. As this is not the case for the models studied later, it is omitted here.

Respectively, the linear measurement models are given by

$$\mathbf{y}_i(k) = \mathbf{H}_i\mathbf{x}(k) + \mathbf{v}_i(k) \tag{2}$$

where $\mathbf{y}_i(k)$ is the observation vector of the ith sensor, $i = 1,\ldots,N$. $\mathbf{H}_i$ is the corresponding measurement matrix and $\mathbf{v}_i(k)$ a zero-mean, white noise sequence with covariance matrix $\mathbf{R}_i(k)$ representing the measurement noise. To avoid stability issues [28], we assume for simplicity that every sensor is able to measure the complete position of the target and, thus, that the system is fully observable. Furthermore, only one easily detectable target shall be present in the scene without any clutter so that the task of data association is trivial.

According to these model equations, the *Centralized* KF (CKF) algorithm with multiple inputs in its information form can be described as recursively performing the following two steps to calculate the overall state estimate $\hat{\mathbf{x}}_{\mathrm{CKF}}(k \mid k)$ and error covariance matrix $\mathbf{P}_{\mathrm{CKF}}(k \mid k)$ at time instant k [3]:

1. Prediction

$$\hat{\mathbf{x}}_{\mathrm{CKF}}(k \mid k-1) = \mathbf{F}\hat{\mathbf{x}}_{\mathrm{CKF}}(k-1 \mid k-1) \tag{3}$$

$$\mathbf{P}_{\mathrm{CKF}}(k \mid k-1) = \mathbf{F}\mathbf{P}_{\mathrm{CKF}}(k-1 \mid k-1)\mathbf{F}^T + \mathbf{Q}(k-1). \tag{4}$$

2. Estimate correction

$$\hat{\mathbf{x}}_{\mathrm{CKF}}(k \mid k) = \mathbf{P}_{\mathrm{CKF}}(k \mid k)\left(\mathbf{P}^{-1}_{\mathrm{CKF}}(k \mid k-1)\hat{\mathbf{x}}_{\mathrm{CKF}}(k \mid k-1) + \sum_{i=1}^{N}\mathbf{H}_i^T\mathbf{R}_i^{-1}(k)\mathbf{y}_i(k)\right) \tag{5}$$

$$\mathbf{P}^{-1}_{\mathrm{CKF}}(k \mid k) = \mathbf{P}^{-1}_{\mathrm{CKF}}(k \mid k-1) + \sum_{i=1}^{N}\mathbf{H}_i^T\mathbf{R}_i^{-1}(k)\mathbf{H}_i. \tag{6}$$

This is called the information form as the inverse of the covariance matrix $\mathbf{P}^{-1}$ is a measure for the accuracy of the corresponding state estimate $\hat{\mathbf{x}}$ and thus for the information contained in it. Accordingly, $\mathbf{P}^{-1}(k \mid k-1)$ determines the weight given to $\hat{\mathbf{x}}(k \mid k-1)$ in (5).

In the *Decentralized* KF (DKF), Local Kalman Filters (LKFs) produce estimates $\hat{\mathbf{x}}_i(k \mid k)$ based on the information available from a single sensor i using the standard KF equations, i.e., (3)–(6) with $N = 1$. At a Fusion Center (FC), these estimates are fused together to form the overall state estimate $\hat{\mathbf{x}}_{\mathrm{DKF}}(k \mid k)$ [22]:

$$\hat{\mathbf{x}}_{\mathrm{DKF}}(k \mid k) = \mathbf{P}_{\mathrm{DKF}}(k \mid k)\left(\mathbf{P}^{-1}_{\mathrm{DKF}}(k \mid k-1)\hat{\mathbf{x}}_{\mathrm{DKF}}(k \mid k-1) + \sum_{i=1}^{N}[\mathbf{P}_i^{-1}(k \mid k)\hat{\mathbf{x}}_i(k \mid k) - \mathbf{P}_i^{-1}(k \mid k-1)\hat{\mathbf{x}}_i(k \mid k-1)]\right) \tag{7}$$

$$\mathbf{P}^{-1}_{\mathrm{DKF}}(k \mid k) = \mathbf{P}^{-1}_{\mathrm{DKF}}(k \mid k-1) + \sum_{i=1}^{N}[\mathbf{P}_i^{-1}(k \mid k) - \mathbf{P}_i^{-1}(k \mid k-1)] \tag{8}$$

where $\mathbf{P}_{\mathrm{DKF}}$ and $\mathbf{P}_i$ are the error covariance matrices of the state estimates $\hat{\mathbf{x}}_{\mathrm{DKF}}$ at the FC and $\hat{\mathbf{x}}_i$ at the LKFs, respectively.

The state estimate $\hat{\mathbf{x}}_{\mathrm{DKF}}(k \mid k)$ in (7) can easily be shown to be equivalent to $\hat{\mathbf{x}}_{\mathrm{CKF}}(k \mid k)$ in (5): Solving (5) in the single sensor case, i.e., $N = 1$, for the weighted measurement $\mathbf{H}_i^T \mathbf{R}_i^{-1}(k)\mathbf{y}_i(k)$ leads to the equivalence between $\mathbf{H}_i^T \mathbf{R}_i^{-1}(k)\mathbf{y}_i(k)$ in (5) and the gain in information between the predicted local estimates $\hat{\mathbf{x}}_i(k \mid k-1)$ and the corrected ones $\hat{\mathbf{x}}_i(k \mid k)$ in (7)

$$\mathbf{H}_i^T \mathbf{R}_i^{-1}(k)\mathbf{y}_i(k) = \mathbf{P}_i^{-1}(k \mid k)\hat{\mathbf{x}}_i(k \mid k) - \mathbf{P}_i^{-1}(k \mid k-1)\hat{\mathbf{x}}_i(k \mid k-1). \quad (9)$$

Therefore, it is not the information contained in the local estimates itself but the gain in information that counts.

3. BANDWIDTH REQUIREMENTS

Looking at (7) and (8), it is sensible to save bandwidth in a DKF by directly transmitting the vector[1]

$$\Delta\hat{\mathbf{x}}_{\mathrm{weighted},i}(k) := \mathbf{P}_i^{-1}(k \mid k)\hat{\mathbf{x}}_i(k \mid k) - \mathbf{P}_i^{-1}(k \mid k-1)\hat{\mathbf{x}}_i(k \mid k-1) \quad (10)$$

and the matrix

$$\Delta\mathbf{I}_i(k) := \mathbf{P}_i^{-1}(k \mid k) - \mathbf{P}_i^{-1}(k \mid k-1) \quad (11)$$

instead of $\mathbf{P}_i^{-1}(k \mid k)$, $\hat{\mathbf{x}}_i(k \mid k)$, $\mathbf{P}_i^{-1}(k \mid k-1)$ and $\hat{\mathbf{x}}_i(k \mid k-1)$. This not only saves half of the communication bandwidth but also processing power at the FC.

Despite these savings, the bandwidth required by a distributed fusion network may still be higher compared with a centralized architecture, as the information packages are usually larger due to the state vector being of a higher dimension than the measurement vector. On the other hand, mislocalizations due to clutter are filtered out locally and need not be transmitted. Furthermore, many sensors do not provide position measurements of the object directly but merely scan the scene, like e.g., laser-radars. In this case, the bandwidth requirements would increase dramatically if the measurements were not preprocessed locally and, thus, a distributed fusion architecture lends itself naturally.

For a large system with many sensors, it is also likely that the central processor or the communication network are not able to handle the large amount of data transmitted by the sensors. In this case, centralized fusion is no longer applicable except if a corresponding amount of measurements is discarded completely. This is, however, likely to affect the estimation performance severely if no smart communications resource management techniques are applied [24]. In this case, distributed fusion opens up the possibility to distribute the processing load and to save the necessary bandwidth by letting the fusion nodes communicate less frequently.

Additionally, solar and battery powered sensors without wiring have become popular recently as they are easy to install [5, 13]. Due to their limited energy resources, it is important to save transmission energy even if sufficient bandwidth is available. The economical usage of transmission energy will become even more important in the future as the performance of microprocessors increases continuously according to Moore's law so that they need less and less energy for the same task. The energy needed for the transmission of the data is, however, mostly unaffected by these improvements [5].

Finally, it is sensible to adapt the reduction in communication rate to the movement of the tracked target. If the object is stationary or if it moves with a nearly constant velocity, its future state can be predicted more reliably and the communication rate can be reduced further than for a maneuvering target [9].

4. REDUCED COMMUNICATION RATE

As far as the DKF is concerned, reducing the communication rate at which information packages are sent from the LKFs to the FC by a factor m results in all predictions by one step being replaced with predictions by m steps in (7) and (8):

$$\hat{\mathbf{x}}_{\mathrm{DKF}_m}(k \mid k) = \mathbf{P}_{\mathrm{DKF}_m}(k \mid k) \left(\mathbf{P}^{-1}_{\mathrm{DKF}_m}(k \mid k-m)\hat{\mathbf{x}}_{\mathrm{DKF}_m}(k \mid k-m) + \sum_{i=1}^{N} [\mathbf{P}_i^{-1}(k \mid k)\hat{\mathbf{x}}_i(k \mid k) - \mathbf{P}_i^{-1}(k \mid k-m)\hat{\mathbf{x}}_i(k \mid k-m)] \right) \quad (12)$$

$$\mathbf{P}^{-1}_{\mathrm{DKF}_m}(k \mid k) = \mathbf{P}^{-1}_{\mathrm{DKF}_m}(k \mid k-m) + \sum_{i=1}^{N} (\mathbf{P}_i^{-1}(k \mid k) - \mathbf{P}_i^{-1}(k \mid k-m)). \quad (13)$$

Any other communication issues are ignored for simplicity. Like in Section 2, it is still assumed that all sensors run synchronously and that information packages travel over communication links without any delay. Furthermore, the update rate at the LKFs is not affected. The LKFs still run at the sensor observation rate.

Unfortunately, if the predictions by one step are replaced by predictions by m steps, the gain in information is no longer based on one measurement but on m measurements and $m-1$ predictions. As these $m-1$ predictions are subject to the same process noise in all LKFs, the gain in information of the different LKFs is no longer statistically independent.

[1] "$x := \ldots$" means "x is defined as $\ldots$".

As this statistical dependence is not taken into account during the fusion process in the FC, the performance of the DKF degrades for such a reduced communication rate [10, 22]. On the other hand, if $\mathbf{w}(k) \equiv 0$, i.e., the target's dynamics can be modeled exactly, the local estimates $\hat{\mathbf{x}}_i(k \mid k)$ are not correlated and, therefore, the communication rate can be reduced at will without any performance degradation.

For less and less frequent communication between the LKFs and the FC, i.e., $m \to \infty$, the information contained in the predicted state estimates becomes less and less reliable. This is represented by the inverses of the corresponding error covariance matrices $\mathbf{P}^{-1}_{\mathrm{DKF}}(k \mid k-m)$ and $\mathbf{P}_i^{-1}(k \mid k-m)$ approaching zero. Thus, no weight is given to these estimates and they can be discarded in (12) and (13) leading to

$$\hat{\mathbf{x}}_{\mathrm{naïve}}(k \mid k) = \mathbf{P}_{\mathrm{naïve}}(k \mid k) \sum_{i=1}^{N} \mathbf{P}_i^{-1}(k \mid k) \hat{\mathbf{x}}_i(k \mid k) \tag{14}$$

$$\mathbf{P}^{-1}_{\mathrm{naïve}}(k \mid k) = \sum_{i=1}^{N} \mathbf{P}_i^{-1}(k \mid k). \tag{15}$$

This is equivalent to the so-called naïve fusion architecture that assumes the local state estimates $\hat{\mathbf{x}}_i(k \mid k)$ and $\hat{\mathbf{x}}_j(k \mid k)$ to be statistically independent for all $i \neq j$.

As a consequence, $m \to \infty$ would result in a system where infinite intervals lie between two communication cycles so that no data would ever be transmitted. The performance of this hypothetical system can, however, readily be determined using the naïve fusion architecture whose track estimate can be formed for every time instant k, i.e., at the sensor observation rate.

From a different perspective, this somewhat astonishing finding can be explained as follows: As already stated, the local state estimates are statistically dependent due to propagating the same underlying process noise. This statistical dependence is properly corrected for in the DKF of (7) and (8) by the term

$$\mathbf{X}_{\mathrm{DKF}}(k \mid k-1) := \mathbf{P}^{-1}_{\mathrm{DKF}}(k \mid k-1) \hat{\mathbf{x}}_{\mathrm{DKF}}(k \mid k-1) - \sum_{i=1}^{N} \mathbf{P}_i^{-1}(k \mid k-1) \hat{\mathbf{x}}_i(k \mid k-1). \tag{16}$$

In the DKF_m of (12) and (13), this term is approximated by

$$\mathbf{X}_{\mathrm{DKF}_m}(k \mid k-m) := \mathbf{P}^{-1}_{\mathrm{DKF}_m}(k \mid k-m) \hat{\mathbf{x}}_{\mathrm{DKF}_m}(k \mid k-m) - \sum_{i=1}^{N} \mathbf{P}_i^{-1}(k \mid k-m) \hat{\mathbf{x}}_i(k \mid k-m) \tag{17}$$

and the $\mathrm{DKF}_{\mathrm{naïve}}$ of (14) and (15) neglects the statistical dependence completely, i.e., $\mathbf{X}_{\mathrm{DKF}_{\mathrm{naïve}}}(k \mid 0) \equiv 0$. Therefore, it can serve as a worst case scenario for such a reduction in communication rate, i.e., the estimate $\hat{\mathbf{x}}_{\mathrm{naïve}}(k \mid k)$ in (14) is always less accurate than $\hat{\mathbf{x}}_{\mathrm{DKF}_m}(k \mid k)$ in (12), for all values of m.

Finally, it should be noted that $\mathbf{P}_{\mathrm{DKF}}$ is a valid estimate of the mean square error as it is an optimal Kalman filter. This is, however, neither true for $\mathbf{P}_m$ nor for $\mathbf{P}_{\mathrm{naïve}}$ (except for $\mathbf{w}(k) \equiv 0$). As the DKF_m and the $\mathrm{DKF}_{\mathrm{naïve}}$ ignore the correlation between the local estimates at least partially, they overestimate their own performance, i.e.,

$$\begin{aligned} \mathbf{P}_{\mathrm{naïve}} \leq \mathbf{P}_{\mathrm{DKF}_m} \leq \mathbf{P}_{\mathrm{DKF}} &= \mathrm{E}\{\tilde{\mathbf{X}}_{\mathrm{DKF}} \tilde{\mathbf{X}}^T_{\mathrm{DKF}}\} \\ &\leq \mathrm{E}\{\tilde{\mathbf{X}}_{\mathrm{DKF}_m} \tilde{\mathbf{X}}^T_{\mathrm{DKF}_m}\} \leq \mathrm{E}\{\tilde{\mathbf{X}}_{\mathrm{naïve}} \tilde{\mathbf{X}}^T_{\mathrm{naïve}}\} \end{aligned} \tag{18}$$

where $\tilde{\mathbf{x}}_*(k \mid k) = \hat{\mathbf{x}}_*(k \mid k) - \mathbf{x}(k)$ and "$\mathbf{A} \leq \mathbf{B}$" means that the difference $\mathbf{B} - \mathbf{A}$ is positive semidefinite. The relationship in (18) is valid for "$(k \mid k)$" as well as "$(k \mid k-1)$".

For complex systems containing several hierarchies or even feedback loops, this inconsistency between estimated and true error covariance matrix can build up and cause stability problems. Furthermore, it may cause problems during the association of the measurements to the tracked objects.

5. PERFORMANCE ANALYSIS

In this section, the performance degradation due to infrequent communication is investigated in detail. First, the performance of the $\mathrm{DKF}_{\mathrm{naïve}}$ defined by (14) and (15) is derived theoretically. As detailed in Section 4, it presents an upper bound on the performance degradation for a reduction in communication rate, as it ignores the correlation between the local estimates completely. Its performance is equivalent to a hypothetical system where infinite intervals lie between two communication cycles, i.e., $m \to \infty$. Second, the theoretical performance degradation is compared with simulative results. Finally, a simulative study concerning the performance of the DKF_m of (12) and (13) is conducted for realistic reductions in the communication rate $m \ll \infty$.

5.1. Theoretical Analysis of $\mathrm{DKF}_{\mathrm{naïve}}$

The theoretical performance of the $\mathrm{DKF}_{\mathrm{naïve}}$ defined by (14) and (15) can be derived as follows. Introducing $\tilde{\mathbf{x}}_*(k \mid k) = \hat{\mathbf{x}}_*(k \mid k) - \mathbf{x}(k)$ in (14) leads to

$$\begin{aligned} \mathbf{P}^{-1}_{\mathrm{naïve}}(k \mid k) \tilde{\mathbf{x}}_{\mathrm{naïve}}(k \mid k) &= \sum_{i=1}^{N} \mathbf{P}_i^{-1}(k \mid k) \tilde{\mathbf{x}}_i(k \mid k) \\ &\quad - \left[\mathbf{P}^{-1}_{\mathrm{naïve}}(k \mid k) - \sum_{i=1}^{N} \mathbf{P}_i^{-1}(k \mid k) \right] \mathbf{x}(k). \end{aligned} \tag{19}$$

According to (15), the second term is zero. Therefore, the true error covariance matrix $\mathbf{P}_{\mathrm{true}}(k \mid k) :=$

$\mathrm{E}\{\tilde{\mathbf{x}}_{\text{naïve}}(k \mid k)\tilde{\mathbf{x}}^T_{\text{naïve}}(k \mid k)\}$ of the $\mathrm{DKF}_{\text{naïve}}$ satisfies

$$\mathbf{P}^{-1}_{\text{naïve}}(k \mid k)\mathbf{P}_{\text{true}}(k \mid k)\mathbf{P}^{-1}_{\text{naïve}}(k \mid k) = \sum_{i=1}^{N}\left(\mathbf{P}_i^{-1}(k \mid k) + \sum_{j=1 j\neq i}^{N}\mathbf{P}_i^{-1}(k \mid k)\boldsymbol{\Sigma}_{i,j}(k \mid k)\mathbf{P}_j^{-1}(k \mid k)\right) \tag{20}$$

where the cross-covariance $\boldsymbol{\Sigma}_{i,j}(k \mid k)$ between two local estimates $\hat{\mathbf{x}}_i(k \mid k)$ and $\hat{\mathbf{x}}_j(k \mid k)$ can be determined using the following equation [1]

$$\boldsymbol{\Sigma}_{i,j}(k \mid k) = (\mathbf{I} - \mathbf{K}_i(k)\mathbf{H}_i)\cdot(\mathbf{F}\boldsymbol{\Sigma}_{i,j}(k-1 \mid k-1)\mathbf{F}^T + \mathbf{Q}) \cdot(\mathbf{I} - \mathbf{K}_j(k)\mathbf{H}_j)^T. \tag{21}$$

$\mathbf{K}_i(k)$ and $\mathbf{K}_j(k)$ denote the Kalman gains. Using (15) once more, (20) becomes

$$\mathbf{P}_{\text{true}}(k \mid k) = \mathbf{P}_{\text{naïve}}(k \mid k) + \mathbf{P}_{\text{naïve}}(k \mid k) \cdot\left(\sum_{i=1}^{N}\sum_{j=1 j\neq i}^{N}\mathbf{P}_i^{-1}(k \mid k)\boldsymbol{\Sigma}_{i,j}(k \mid k)\mathbf{P}_j^{-1}(k \mid k)\right)\mathbf{P}_{\text{naïve}}(k \mid k). \tag{22}$$

Therefore, the inconsistency of (18) between the true covariance matrix $\mathbf{P}_{\text{true}} = \mathrm{E}\{\tilde{\mathbf{x}}_{\text{naïve}}(k \mid k)\tilde{\mathbf{x}}^T_{\text{naïve}}(k \mid k)\}$ and the estimated covariance matrix $\mathbf{P}_{\text{naïve}}$ consists in the term depending on the cross-covariance $\boldsymbol{\Sigma}_{i,j}$ between the local estimates.

The case of identical sensors, i.e., $\mathbf{P}_i(k \mid k) = \mathbf{P}_{\text{LKF}}(k \mid k)\ \forall i$, also results in $\boldsymbol{\Sigma}_{i,j}(k \mid k) = \boldsymbol{\Sigma}_{j,i}(k \mid k) = \boldsymbol{\Sigma}_{\text{LKFs}}(k \mid k)\ \forall i, j$. Therefore, the true error covariance matrix simplifies to

$$\begin{aligned}\mathbf{P}_{\text{true}}(k \mid k) &= \mathbf{P}_{\text{naïve}}(k \mid k) + N(N-1)\mathbf{P}_{\text{naïve}}(k \mid k) \cdot\mathbf{P}^{-1}_{\text{LKF}}(k \mid k)\boldsymbol{\Sigma}_{\text{LKFs}}(k \mid k)\mathbf{P}^{-1}_{\text{LKF}}(k \mid k)\mathbf{P}_{\text{naïve}}(k \mid k)\\ &= \mathbf{P}_{\text{naïve}}(k \mid k) + \frac{N-1}{N}\boldsymbol{\Sigma}_{\text{LKFs}}(k \mid k)\end{aligned} \tag{23}$$

as $\mathbf{P}_{\text{naïve}}(k \mid k) = (1/N)\mathbf{P}_{\text{LKF}}(k \mid k)$.

The evaluation of (22) and (23) is straightforward compared with the solution of the asymmetric Lyapunov equation in [10] describing the steady state performance of a DKF for arbitrary communication rates, as the latter consists of several non-trivial systems of linear equations. A further advantage consists in the fact that the term depending on the cross-covariance $\boldsymbol{\Sigma}_{i,j}$ in (22) and (23) represents an explicit explanation for the inconsistency of the naïve fusion architecture.

5.2. Simulative Analysis of $\mathrm{DKF}_{\text{naïve}}$

In addition to validating the theoretical analysis of the $\mathrm{DKF}_{\text{naïve}}$, the following simulative study shall provide some quantitative numbers for its performance degradation and its inconsistency in typical tracking scenarios. In contrast to [10], the study not only covers a nearly constant velocity but also a nearly constant acceleration model for the target dynamics. The results lead to a generalization of the target maneuvering index [3], which is commonly used as the decisive parameter for describing the performance of a Kalman filter. For simplicity the comparison is restricted to the steady state.

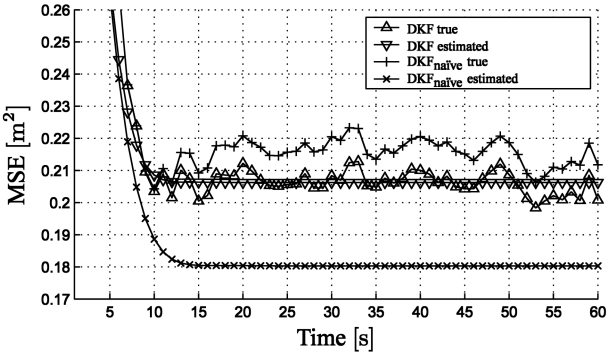

Fig. 1. Comparison between true and estimated MSE of DKF and $\mathrm{DKF}_{\text{naïve}}$ ($q_{\text{NCV}} = 0.01\mathrm{m}^2/(\mathrm{s}^3)$, $T_s = 1$ s, $\sigma_v = 1$ m).

5.2.1. Nearly Constant Velocity

First, $N = 2$ sensors track a target whose one-dimensional dynamics can be described by the following Nearly Constant Velocity (NCV) model [3]

$$\begin{bmatrix}x(k+1)\\ \dot{x}(k+1)\end{bmatrix} = \begin{bmatrix}1 & T_s\\ 0 & 1\end{bmatrix}\begin{bmatrix}x(k)\\ \dot{x}(k)\end{bmatrix} + \mathbf{w}_{\text{NCV}}(k) \tag{24}$$

where the process noise is given by

$$\mathbf{w}_{\text{NCV}}(k) = \int_0^{T_s}\begin{bmatrix}T_s - t\\ 1\end{bmatrix}u_{\text{NCV}}(kT_s + t)dt \tag{25}$$

and $u_{\text{NCV}}(t)$ is zero-mean continuous random noise with power spectral density q_{NCV}, leading to the following process noise covariance matrix

$$\mathbf{Q}_{\text{NCV}} = \begin{bmatrix}\frac{1}{3}T_s^3 & \frac{1}{2}T_s^2\\ \frac{1}{2}T_s^2 & T_s\end{bmatrix}q_{\text{NCV}}. \tag{26}$$

The measurements $y_i(k)$ are the position in Cartesian coordinates

$$y_i(k) = x(k) + v_i(k), \qquad i = 1, 2 \tag{27}$$

with variances $\sigma^2_{v,i}$.

Fig. 1 presents the comparison between the true and estimated Mean Square Error (MSE)

$$\mathrm{MSE} \approx \mathrm{E}\{(\hat{x}_*(k \mid k) - x(k))^2\} \tag{28}$$

of the position component in $\hat{\mathbf{x}}_{\text{DKF}}(k \mid k)$ of (7) and $\hat{\mathbf{x}}_{\text{naïve}}(k \mid k)$ of (14) for a typical example, where $q_{\text{NCV}} = 0.01\mathrm{m}^2/(\mathrm{s}^3)$, $T_s = 1$ s and $\sigma_v = 1$ m. The "true" MSEs are thereby averaged on 5000 Monte Carlo runs. In accordance with (18), it can be seen how the DKF slightly outperforms the $\mathrm{DKF}_{\text{naïve}}$ by approximately 4%. Furthermore, the DKF estimates its accuracy correctly

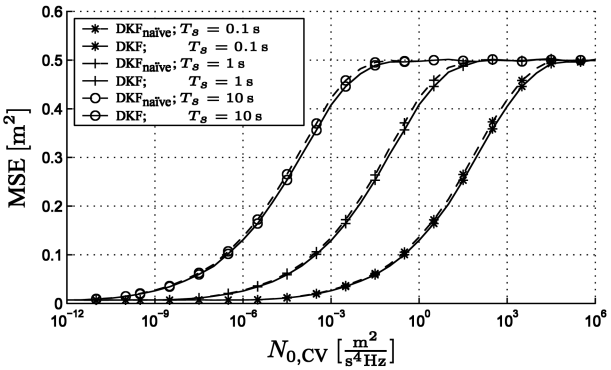

Fig. 2. Comparison between $\mathrm{MSE}_{\mathrm{naïve}}$ and $\mathrm{MSE}_{\mathrm{DKF}}$ as a function of the process noise q_{NCV} (σ_v = 1 m).

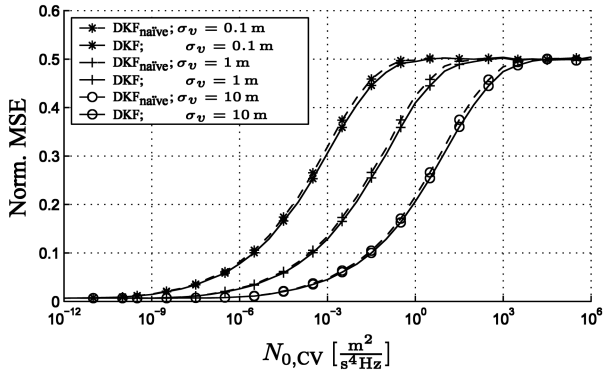

Fig. 3. Comparison between $\mathrm{MSE}_{\mathrm{naïve}}$ and $\mathrm{MSE}_{\mathrm{DKF}}$ normalized by σ_v^2 as a function of the process noise q_{NCV} (T_s = 1 s).

whereas the $\mathrm{DKF}_{\mathrm{naïve}}$ produces estimates of its MSE that are about 16% more accurate (smaller) as compared to the DKF_m even though its true MSE is slightly worse.

Fig. 2 displays the true MSEs of DKF and $\mathrm{DKF}_{\mathrm{naïve}}$ averaged over time as a function of the process noise q_{NCV} for three different sampling periods T_s = 0.1 s, 1 s, 10 s and a measurement noise σ_v = 1 m. Fig. 3 shows the corresponding comparison for varying σ_v = 0.1 m, 1 m, 10 m and T_s = 1 s. To allow for a comparison, the MSEs are normalized by σ_v^2 this time. For every point on each line, 1000 Monte Carlo runs with 400 measurements per simulation were performed. To obtain an estimate of the steady state performance, the averages are only based on the last 200 measurements.

For high values of q_{NCV}, the curves in both figures approach the variance of the combined measurements $\sigma_{v,\mathrm{comb}}^2 = \sigma_{v,1}^2\sigma_{v,2}^2/(\sigma_{v,1}^2 + \sigma_{v,2}^2) = 0.5\sigma_v^2$. For low values of q_{NCV}, they should approach zero as KFs are able to estimate the position arbitrarily precisely if no process noise is present and if a sufficient number of observations is available. Due to a finite number of observations, this is not the case here.

In both Figs. 2 and 3, changing the parameter merely results in a shift of the corresponding curves. Their shape is not affected. If T_s is increased by a factor of 10, q_{NCV} needs to be decreased by a factor of 1000 to obtain the same results. On the other hand, if σ_v is increased by a factor of 10, q_{NCV} needs to be increased by a factor of 100.

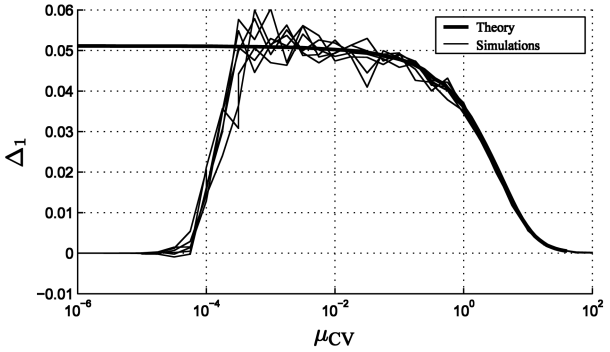

Fig. 4. Relative difference Δ_1 between $\mathrm{MSE}_{\mathrm{naïve}}$ and $\mathrm{MSE}_{\mathrm{DKF}}$ as a function of the target maneuvering index μ_{NCV}.

Therefore, using the target maneuvering index [3]

$$\mu_{\mathrm{NCV}} := \sqrt{\frac{q_{\mathrm{NCV}}T_s^3}{\sigma_v^2}} \tag{29}$$

as independent variable leads to an invariance against a variation in the sampling period T_s and the measurement noise σ_v. This can be seen in Fig. 4, which shows the relative difference[2]

$$\Delta_1 = \frac{\mathrm{MSE}_{\mathrm{naïve}} - \mathrm{MSE}_{\mathrm{DKF}}}{\mathrm{MSE}_{\mathrm{DKF}}} \stackrel{!}{\equiv} \frac{P_{\mathrm{true}}^{(1,1)} - P_{\mathrm{DKF}}^{(1,1)}}{P_{\mathrm{DKF}}^{(1,1)}} \tag{30}$$

between the six corresponding dashed and solid curve pairs in Figs. 2 and 3. The identity with the right-hand side follows from the definition of $\mathbf{P}_{\mathrm{true}}$ in (23) and the fact that the DKF estimates its accuracy correctly. This analytical prediction of Δ_1 is represented by the bold line.

For large values of μ_{NCV}, the different curves all approach zero. This can be explained by the predicted states $\hat{\mathbf{x}}_i(k \mid k-1)$ being not only correlated but also unreliable in this case. As large values of μ_{NCV} also imply a large process noise q, the predicted states are given almost no weight compared with the measurements $y_i(k)$ in calculating $\hat{\mathbf{x}}_i(k \mid k)$ in the LKFs. Note that the Kalman filters are of little use in this case.

For small values of μ_{NCV}, (23) predicts Δ_1 to approach 5.1% asymptotically, whereas the simulations show Δ_1 to approach zero. This significant difference can be explained by the analytical curve predicting the steady state behavior, whereas the steady state is never reached during the simulations for such small values of μ_{NCV}. As described by (21) and as depicted in Fig. 5, the cross-covariance $\mathbf{\Sigma}_{i,j}(k \mid k)$ between the local estimates rises only slowly for low values of μ_{NCV}. Therefore, the estimates $\hat{\mathbf{x}}_{\mathrm{DKF}}(k \mid k)$ and $\hat{\mathbf{x}}_{\mathrm{naïve}}(k \mid k)$ are quasi identical and Δ_1 equals zero during the initialization phase.

[2]"$\{!\}$ over $\{\equiv, =, <, >\}$" means "shall be" or "needs to be." Furthermore, the superscript (1,1) denotes the upper-left element of the matrix.

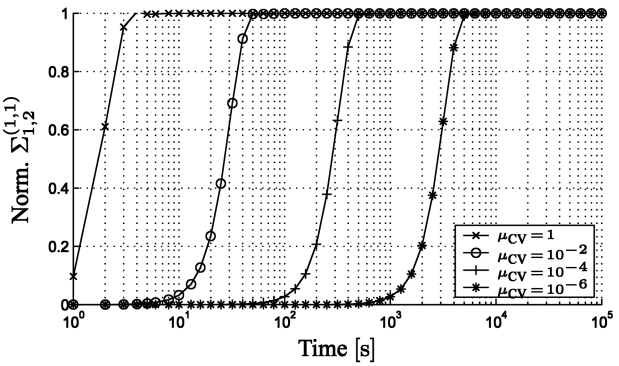

Fig. 5. Time dependency of the normalized cross-covariance between the local position estimates.

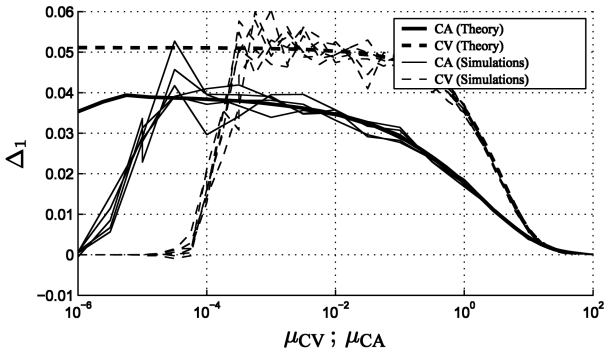

Fig. 6. Relative difference Δ_1 between $\text{MSE}_{\text{naïve}}$ and MSE_{DKF} as a function of the target maneuvering index μ.

5.2.2. Nearly Constant Acceleration

In this section, the previous analysis is extended to a Nearly Constant Acceleration (NCA) model being used for the target dynamics, i.e.,

$$\begin{bmatrix} x(k+1) \\ \dot{x}(k+1) \\ \ddot{x}(k+1) \end{bmatrix} = \begin{bmatrix} 1 & T_s & \frac{1}{2}T_s^2 \\ 0 & 1 & T_s \\ 0 & 0 & 1 \end{bmatrix} \begin{bmatrix} x(k) \\ \dot{x}(k) \\ \ddot{x}(k) \end{bmatrix} + \mathbf{w}_{\text{NCA}}(k) \tag{31}$$

where the process noise is given by

$$\mathbf{w}_{\text{NCA}}(k) = \int_0^{T_s} \begin{bmatrix} \frac{1}{2}(T_s - t)^2 \\ T_s - t \\ 1 \end{bmatrix} u_{\text{NCA}}(kT_s + t)dt \tag{32}$$

and $u_{\text{NCA}}(t)$ is a zero-mean continuous random noise signal with power spectral density q_{NCA}, leading to the following process noise covariance matrix

$$\mathbf{Q}_{\text{NCA}} = \begin{bmatrix} \frac{1}{20}T_s^5 & \frac{1}{8}T_s^4 & \frac{1}{6}T_s^3 \\ \frac{1}{8}T_s^4 & \frac{1}{3}T_s^3 & \frac{1}{2}T_s^2 \\ \frac{1}{6}T_s^3 & \frac{1}{2}T_s^2 & T_s \end{bmatrix} q_{\text{NCA}}. \tag{33}$$

Fig. 6 shows the relative difference Δ_1 between the true MSEs of the $\text{DKF}_{\text{naïve}}$ and the DKF for the NCV and the NCA model. For the latter, the target maneuvering index is defined as [3]

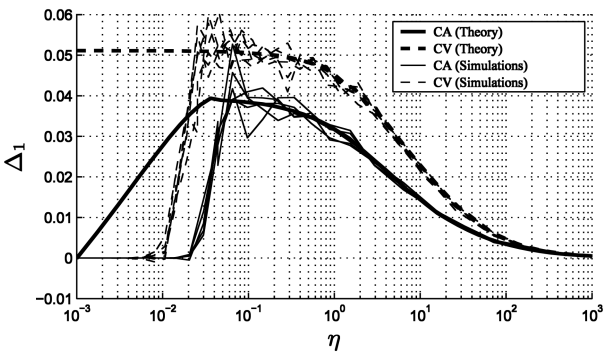

Fig. 7. Relative difference Δ_1 between $\text{MSE}_{\text{naïve}}$ and MSE_{DKF} as a function of the weighting ratio η.

$$\mu_{\text{NCA}} := \sqrt{\frac{q_{\text{NCA}} T_s^5}{\sigma_v^2}}. \tag{34}$$

Like in the nearly constant velocity case, the curves are invariant against a variation in T_s and σ_v. On the other hand, the curves for the two different target models clearly do not match.

A comparison between the definitions of the target maneuvering indices in (29) and (34) and the respective process noise covariance matrices in (26) and (33) reveals that μ^2 is proportional to the ratio $Q^{(1,1)}/\sigma_v^2$ between the variance of the predicted position estimate *due to the process noise* and the variance of the measurement. Therefore, μ is an indicator for how much weight is given to the measurement and the predicted estimate during the track update in the LKFs, respectively (see (5) with $N = 1$).

On the other hand, as described in (4), the accuracy of the prediction in the LKFs does not only depend on the covariance of the process noise $\mathbf{Q}$ but also on the state transition matrix $\mathbf{F}$ and the inaccuracy of the last estimate $\mathbf{P}(k-1 \mid k-1)$. The correct ratio

$$\eta := \frac{P^{(1,1)}_{\text{LKF, pred}}}{\sigma_v^2} \tag{35}$$

between the weight given to the measurement and the weight given to the predicted position estimate can be taken from the simulations. For the case of a NCV and a NCA model, it can, however, also be calculated for the steady state by numerically solving a system of nonlinear equations (as detailed in the Appendix).

The resulting curves for the relative difference Δ_1 as a function of η are displayed in Fig. 7, where the bold lines again present the analytical predictions. This time the curves for the NCV and the NCA model show the same progression. Only the maximum degradation for the NCA model of around 4% is lower than the 5.1% for the NCV model, as also predicted by the theory. This can be explained by the same weighting ratio η being reached for a smaller process noise q for the NCA model. As the common process noise is responsible

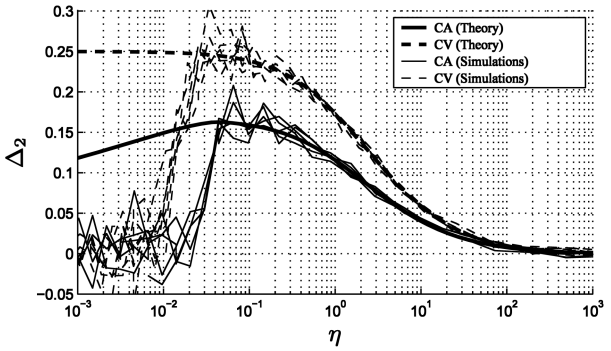

Fig. 8. Relative difference Δ_2 between true and estimated MSE of $\mathrm{DKF}_{\mathrm{naïve}}$ as a function of the weighting ratio η.

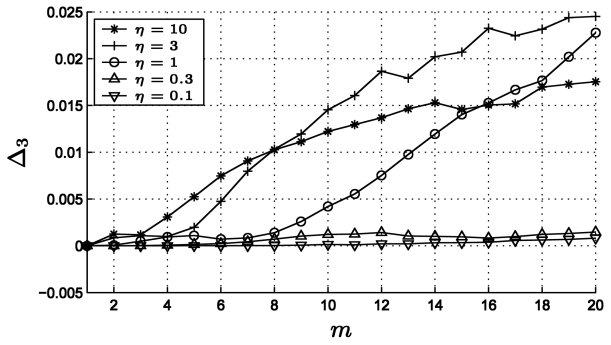

Fig. 9. Relative difference Δ_3 between $\mathrm{MSE}_{\mathrm{DKF}_m}$ and $\mathrm{MSE}_{\mathrm{DKF}}$ as a function of the the update rate m for the nearly constant velocity model (T_s = 1 s, σ_v = 1 m).

for the correlation between the local estimates, the correlation is also lower for the NCA model.

Note that for small values of η even the analytical prediction fails for the NCA model. This is due to the numerical solution of the system of non-linear equations, which is needed to determine the steady state performance of the KFs, reaching its limits for such small values. Simulations with 10000 measurements indicate that Δ_1 stays at its maximum also in the NCA case.

KFs do not only produce state estimates $\hat{\mathbf{x}}$ but also calculate an accuracy of these estimates in form of the error covariance matrix $\mathbf{P}$. As stated earlier, the DKF estimates its accuracy correctly whereas the $\mathrm{DKF}_{\mathrm{naïve}}$, although performing slightly worse, estimates its accuracy even better than that of the DKF.

Fig. 8 shows this difference

$$\Delta_2 = \frac{\mathrm{MSE}_{\mathrm{naïve}} - \mathrm{MSE}_{\mathrm{estimated}}}{\mathrm{MSE}_{\mathrm{estimated}}} \stackrel{!}{\equiv} \frac{P^{(1,1)}_{\mathrm{true}} - P^{(1,1)}_{\mathrm{naïve}}}{P^{(1,1)}_{\mathrm{naïve}}} \tag{36}$$

between the true and estimated MSE of the $\mathrm{DKF}_{\mathrm{naïve}}$ as a function of the weighting ratio η. It can be seen how this difference Δ_2 can again be predicted very precisely by (23). The shape of these curves is very similar to those in Fig. 7 for the difference between the true MSE of the $\mathrm{DKF}_{\mathrm{naïve}}$ and the DKF. The maxima are, however, a lot higher at 16% and 25%, respectively. This significant overestimation of its own performance

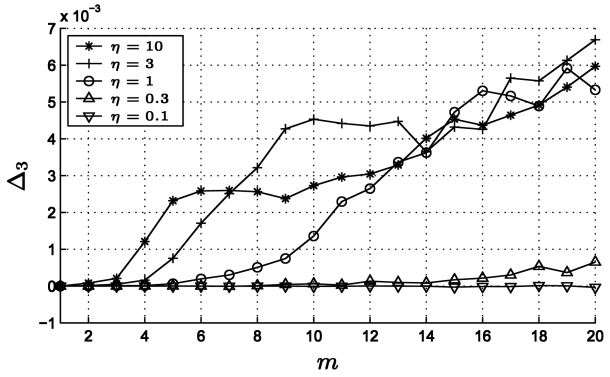

Fig. 10. Relative difference Δ_3 between $\mathrm{MSE}_{\mathrm{DKF}_m}$ and $\mathrm{MSE}_{\mathrm{DKF}}$ as a function of the the update rate m for the nearly constant acceleration model (T_s = 1 s, σ_v = 1 m).

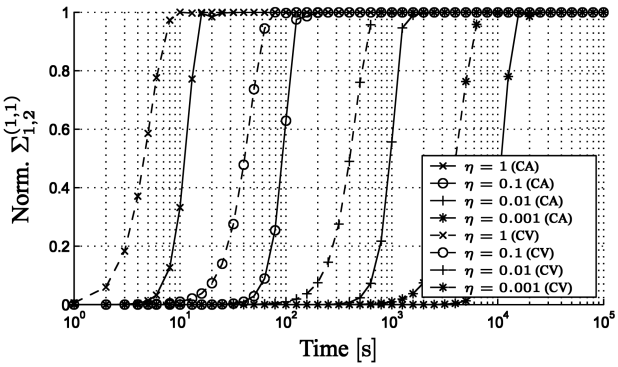

Fig. 11. Time dependency of the normalized cross-covariance between the local position estimates.

in the $\mathrm{DKF}_{\mathrm{naïve}}$ can lead to severe stability problems if the estimates are propagated to other fusion nodes in the system or even fed back to the local estimators.

5.3. Performance Analysis of DKF_m

As already stated, the $\mathrm{DKF}_{\mathrm{naïve}}$ presents an upper bound on the performance degradation for a reduction in communication rate. Its performance is equivalent to a hypothetical system where infinite intervals lie between two communication cycles, i.e., $m \to \infty$. In this section, the performance degradation is examined for realistic reductions in communication rate $m \ll \infty$ using the DKF_m of (12) and (13).

To this end, Figs. 9 and 10 show the relative difference

$$\Delta_3 = \frac{\mathrm{MSE}_{\mathrm{DKF}_m} - \mathrm{MSE}_{\mathrm{DKF}}}{\mathrm{MSE}_{\mathrm{DKF}}} \tag{37}$$

between the MSE of the position component in the state estimate $\hat{\mathbf{x}}_{\mathrm{DKF}_m}(k \mid k)$ of (12) and $\hat{\mathbf{x}}_{\mathrm{DKF}}(k \mid k)$ of (7) as a function of the update rate m for the nearly constant velocity (NCV) and nearly constant acceleration (NCA) model, respectively. The sampling period was set to T_s = 1 s and the measurement noises to σ_v = 1 m. This time 10000 Monte Carlo runs were performed on simulations with 400 measurements.

In both figures, it can be seen that the maximum difference of the $\mathrm{DKF}_{\text{naïve}}$ (see Fig. 7) is not reached in the shown interval $1 \leq m \leq 20$ even for large values of η and that Δ_3 remains almost zero for small values of η. The latter is due to the state vector $\mathbf{x}(k)$ changing only slowly in such scenarios. Therefore, the term $\mathbf{X}_{\mathrm{DKF}_m}(k \mid k-m)$ of (17), which corrects for the statistical dependence between $\hat{\mathbf{x}}_1(k \mid k)$ and $\hat{\mathbf{x}}_2(k \mid k)$ in the DKF_m, stays longer an accurate estimate of the true term $\mathbf{X}_{\mathrm{DKF}}(k \mid k-1)$ of (16) in the DKF.

A comparison between the curves for the NCV and the NCA model shows that those for the NCA model are significantly lower. This can be explained by the maximal degradation being lower, as indicated in Fig. 7, and the maximum cross-covariance also being reached more slowly, as indicated in Fig. 11. The reason for this is again that a smaller process noise q is needed for the same weighting ratio η in the NCA case, and the common process noise being responsible for the correlation between the local estimates.

As a result, it can be concluded that, even for the worst case of $\eta \in [1, 10]$ and the NCV model, the communication rate between the LKFs and the FC can be reduced by at least a factor $m = 8$ without introducing an additional error of more than 1%. For sensors producing measurements at high rates, the error due to infrequent communication is typically even smaller as the short sampling period T_s results in a small target maneuvering index μ and, thus, a small weighting ratio η. Exactly in these scenarios, a reduction in communication rate is most likely to be desirable.

6. CONSERVATIVE FUSION APPROACH

Sophisticated approaches for distributed tracking systems exist that are specifically designed to be robust against unmodeled correlations, like e.g., the covariance intersection method [15] or the bounded covariance inflation method [25]. On the other hand, the results of the last section give rise to a conservative, but simple alternative fusion approach for a reduction in communication rate.

Combining the results of Section 5 with (18) it can be seen that $\mathbf{P}_{\mathrm{DKF}_m}(k \mid k)$ is a slightly too optimistic and $\mathrm{E}\{\tilde{\mathbf{X}}_{\text{naïve}}(k \mid k)\tilde{\mathbf{X}}_{\text{naïve}}(k \mid k)^T\}$ a slightly too conservative estimate of the true accuracy $\mathrm{E}\{\tilde{\mathbf{X}}_{\mathrm{DKF}_m}(k \mid k)\tilde{\mathbf{X}}_{\mathrm{DKF}_m}(k \mid k)^T\}$ of the DKF_m in (12) and (13). As $\mathrm{E}\{\tilde{\mathbf{X}}_{\text{naïve}}(k \mid k)\tilde{\mathbf{X}}_{\text{naïve}}(k \mid k)^T\}$ is equivalent to $\mathbf{P}_{\text{true}}(k \mid k)$, it can be determined using (22) and (23). Therefore, the DKF_m of (12) and (13) can be used without alteration for the estimation of $\hat{\mathbf{x}}_{\mathrm{DKF}_m}(k \mid k)$, i.e., $\mathbf{P}_{\mathrm{DKF}_m}(k \mid k)$ is still used during the recursive estimation. To obtain a conservative estimate, $\mathbf{P}_{\mathrm{DKF}_m}(k \mid k)$ is then simply replaced by $\mathbf{P}_{\text{true}}(k \mid k)$.

The computation of $\mathbf{P}_{\text{true}}(k \mid k)$ in (22) and (23), however, requires the knowledge of $\mathbf{\Sigma}_{i,j}(k \mid k)$ in (21) and, thus, of $\mathbf{K}_i(k)$, for all i and k. In the studied case with a time-invariant state-space representation of the tracking system, the $\mathbf{K}_i(k)$ can simply be (pre-)computed at the FC as they do not depend on the actually observed measurements [3]. In many real-world scenarios, this condition is, however, likely to be violated, like e.g., for a maneuvering target or if the measurement accuracy depends on the distance from the sensor to the target. In this case, the FC may determine the gain sequence at least approximately, in particular if additional information is provided by the LKFs. As (21) is not restricted to the $\mathbf{K}_i(k)$ being the Kalman gains, a predictable sequence of suboptimal filter gains may also be used.

Finally, if the calculation of $\mathbf{P}_{\text{true}}(k \mid k)$ for every time step k shall be avoided, an even more conservative approximation consists in determining the maximum difference $\Delta\mathbf{P}_{\max}$ between $\mathbf{P}_{\text{true}}(k \mid k)$ and $\mathbf{P}_{\text{naïve}}(k \mid k)$, and adding this difference to $\mathbf{P}_{\mathrm{DKF}_m}(k \mid k)$, i.e.,

$$\mathbf{P}_{\mathrm{c}}(k \mid k) = \mathbf{P}_{\mathrm{DKF}_m}(k \mid k) + \Delta\mathbf{P}_{\max}. \tag{38}$$

The difference between $\mathbf{P}_{\text{true}}(k \mid k)$ and $\mathbf{P}_{\text{naïve}}(k \mid k)$ is the term depending on the cross-covariance $\mathbf{\Sigma}_{i,j}(k \mid k)$ between the local estimates in (22) and (23). As the cross-covariance builds up slowly, this term is maximum for the steady state, i.e.,

$$\Delta\mathbf{P}_{\max} = \mathbf{P}_{\text{true}}(\infty \mid \infty) - \mathbf{P}_{\text{naïve}}(\infty \mid \infty). \tag{39}$$

As the Kalman gains $\mathbf{K}_i(\infty)$ are constant, (21) turns into a simple system of linear equations. Consequently, if the $\mathbf{K}_i(\infty)$ can be determined (like e.g., for the NCV and the NCA model), this is also true for $\mathbf{\Sigma}_{i,j}(\infty \mid \infty)$ and, thus, $\Delta\mathbf{P}_{\max}$.

7. CONCLUSIONS

If the communication rate between the Local Kalman Filters (LKFs) and the Fusion Center (FC) needs to be reduced to save communication bandwidth, the performance of the fusion process degrades as the information provided by the different sensors becomes correlated due to propagating the same underlying process noise. A simulative study is performed for a simple system with two local sensors, which are both able to measure the position of the target. It is shown that the ratio η between the weight given to the measurement and the weight given to the predicted position estimate during the track update in the LKFs is more useful in describing the performance degradation than the target maneuvering index. Furthermore, it is found that, even for the worst case of $\eta \in [1, 10]$ and the nearly constant velocity model, the communication rate between the LKFs and the FC can be reduced by at least a factor of 8 without introducing an additional error of more than 1%.

Furthermore, a simple formula for the performance degradation in the worst case of ignoring the correlation due to such a reduction in communication rate completely is derived. As its evaluation is straightforward

compared with the solution of the asymmetric Lyapunov equation for the general case, it can be used for a conservative fusion architecture where the slightly too optimistic state estimates due to such a reduction in communication rate are replaced by slightly too conservative ones.

APPENDIX

In the steady state, the Kalman filter simplifies to

$$\hat{\mathbf{x}}(k \mid k) = \mathbf{F}\hat{\mathbf{x}}(k-1 \mid k-1) + \mathbf{K}(\mathbf{y}(k) - \mathbf{H}_i\hat{\mathbf{x}}(k \mid k-1)) \tag{40}$$

with a constant Kalman gain $\mathbf{K}$. If, as in our case, only the position of the object is measured in 1D, $\mathbf{K}_i$ becomes a vector

$$\mathbf{K}_{\mathrm{NCV}} =: \begin{pmatrix} \alpha \\ \beta/T_s \end{pmatrix} \qquad \text{and} \qquad \mathbf{K}_{\mathrm{NCA}} =: \begin{pmatrix} \alpha \\ \beta/T_s \\ \gamma/T_s^2 \end{pmatrix} \tag{41}$$

in the nearly constant velocity (NCV) and nearly constant acceleration (NCA) case, respectively. Accordingly, the filters are denoted optimal α-β- and α-β-γ-filter [3]. It can easily be shown [26] that

$$\eta := \frac{P_{\mathrm{pred}}^{(1,1)}}{\sigma_v^2} = \frac{\alpha}{1-\alpha}. \tag{42}$$

The corresponding formulas to calculate α and β for a NCV model excited by discretized continuous-time white process noise can be found in [3]:

$$\alpha = \sqrt{2\beta + \frac{\beta^2}{12}} - \frac{\beta}{2} \tag{43}$$

$$\frac{\beta^2}{1-\alpha} = \frac{q_{\mathrm{NCV}}T_s^3}{\sigma_v^2} =: \mu_{\mathrm{NCV}}^2. \tag{44}$$

The following equations for α, β and γ for a NCA model being excited by a discretized continuous-time white process noise can be obtained using the same approach:

$$\beta^2 = 2\alpha\gamma \tag{45}$$

$$\frac{\gamma^2}{120\alpha^2} - \frac{\gamma}{2\alpha} + \frac{4\gamma}{\alpha\beta} - \frac{2\gamma}{\beta} = 1 \tag{46}$$

$$\frac{\gamma^2}{1-\alpha} = \frac{q_{\mathrm{NCA}}T_s^5}{\sigma_v^2} =: \mu_{\mathrm{NCA}}^2. \tag{47}$$

REFERENCES

[1] Y. Bar-Shalom
On the track-to-track correlation problem.
IEEE Transactions on Automatic Control, **26**, 2 (Apr. 1981), 571–572.

[2] Y. Bar-Shalom and L. Campo
The effect of the common process noise on the two-sensor fused-track covariance.
IEEE Transactions on Aerospace and Electronic Systems, **22**, 6 (Nov. 1986), 803–804.

[3] Y. Bar-Shalom and T. Fortmann
Tracking and Data Association.
New York: Academic Press, 1988.

[4] Y. Bar-Shalom, T. Kirubarajan and C. Gokberk
Tracking with classification-aided multiframe data association.
IEEE Transactions on Aerospace and Electronic Systems, **41**, 3 (July 2005), 868–878.

[5] R. R. Brooks
Data Fusion for a Distributed Ground-Based Sensing System.
In D. L. Hall and J. Llinas (Eds.), *Handbook of Multisensor Data Fusion*, Boca Raton: CRC Press, 2001, 25-1–25-9.

[6] N. A. Carlson
Federated square root filter for decentralized parallel processes.
IEEE Transactions on Aerospace and Electronic Systems, **26**, 3 (May 1990), 517–525.

[7] N. A. Carlson
Federated filter for distributed navigation and tracking applications.
In *Proceedings of the ION 58th Annual Meeting/CIGTF 21st Guidance Test Symposium*, June 2002, 340–353.

[8] K. C. Chang, R. K. Saha and Y. Bar-Shalom
On optimal track-to-track fusion.
IEEE Transactions on Aerospace and Electronic Systems, **33**, 4 (Oct. 1997), 1271–1276.

[9] K. C. Chang, X. Yin and R. K. Saha
Evaluating a linear predictive algorithm for bandwidth conservation.
IEEE Transactions on Aerospace and Electronic Systems, **36**, 4 (Oct. 2000), 1407–1414.

[10] K. C. Chang, T. Zhi and R. K. Saha
Performance evaluation of track fusion with information matrix filter.
IEEE Transactions on Aerospace and Electronic Systems, **38**, 2 (Apr. 2002), 455–466.

[11] C.-Y. Chong
Hierarchical estimation.
In *Proceedings of the MIT/ONR Workshop on C3*, July 1979, 205–220.

[12] O. E. Drummond
On track and tracklet fusion filtering.
In *Proceedings of the SPIE Conference on Signal and Data Processing of Small Targets*, 2002, vol. 4728, 176–194.

[13] P. F. Gorder
Sizing up smart dust.
Journal on Computing in Science and Engineering, **5**, 6 (Nov.–Dec. 2003), 6–9.

[14] D. L. Hall and J. Llinas (Eds.)
Handbook of Multisensor Data Fusion.
Boca Raton, FL: CRC Press, 2001.

[15] S. Julier and J. K. Uhlmann
General Decentralized Data Fusion with Covariance Intersection (CI).
In D. L. Hall and J. Llinas (Eds.), *Handbook of Multisensor Data Fusion*, Boca Raton, FL: CRC Press, 2001, 12-1–12-5.

[16] X. R. Li
Unified optimal linear estimation fusion—Part VII: Dynamic systems.
In *Proceedings of the International Conference on Information Fusion* (Fusion), July 2003, 445–462.

[17] X. R. Li and J. Wang
Optimal linear estimation fusion—Part II: Discussions and examples.
In *Proceedings of the International Conference on Information Fusion* (Fusion), July 2000, MoC2-18–MoC2-25.

[18] X. R. Li and K.-S. Zhang
Optimal linear estimation fusion—Part IV: Optimality and efficiency of distributed fusion.
In *Proceedings of the International Conference on Information Fusion* (Fusion), Aug. 2001, WeB1-19–WeB1-26.

[19] X. R. Li, K.-S. Zhang, J. Zhao and Y.-M. Zhu
Optimal linear estimation fusion—Part V: Relationships.
In *Proceedings of the International Conference on Information Fusion* (Fusion), July 2002, 497–504.

[20] X. R. Li and P. Zhang
Unified optimal linear estimation fusion—Part III: Cross-correlation of local estimation errors.
In *Proceedings of the International Conference on Information Fusion* (Fusion), Aug. 2001, WeB1-11–WeB1-18.

[21] X. R. Li, Y.-M. Zhu, J. Wang and C.-Z. Han
Optimal linear estimation fusion—Part I: Unified fusion rules.
IEEE Transactions on Information Theory, **49**, 9 (Sept. 2003), 2192–2208.

[22] M. E. Liggins, C.-Y. Chong, I. Kadar, M. G. Alford, V. Vannicola and S. Thomopoulos
Distributed fusion architectures and algorithms for target tracking.
Proceedings of the IEEE, **85**, 1 (Jan. 1997), 95–107.

[23] E. Nettleton, H. Durrant-Whyte and S. Sukkarieh
A robust architecture for decentralised data fusion.
In *Proceedings of the International Conference on Advanced Robotics* (ICAR), 2003.

[24] D. Nicholson, C. M. Lloyd, S. J. Julier and J. K. Uhlmann
Scalable distributed data fusion.
In *International Conference on Information Fusion* (Fusion), July 2002, vol. 1, 630–635.

[25] S. Reece and S. Roberts
Robust, low-bandwidth, multi-vehicle mapping.
In *International Conference on Information Fusion* (Fusion), 2005.

[26] M. S. Schlosser
Lineare Schätzer zur multisensoriellen Objektverfolgung in verteilten, nichtlinearen Systemen.
Ph.D. thesis, Institut für Nachrichtentechnik, Universität Karlsruhe, 2006.

[27] J. L. Speyer
Computation and transmission requirements for a decentralized linear-quadratic-gaussian control problem.
IEEE Transactions on Automatic Control, **AC-24**, 2 (Apr. 1979), 266–269.

[28] H. Weiss and J. B. Moore
Improved extended Kalman filter design for passive tracking.
IEEE Transactions on Automatic Control, **AC-25**, 4 (Aug. 1980), 807–811.

[29] K.-S. Zhang, X. R. Li, P. Zhang and H.-F. Li
Unified optimal linear estimation fusion—Part VI: Sensor data compression.
In *Proceedings of the International Conference on Information Fusion* (Fusion), July 2003, 221–228.

Markus Schlosser studied electrical engineering at the University of Karlsruhe, Germany, the Ecole Supérieure d'Ingénieurs en Electronique et Electrotechnique (ESIEE) in Paris, France, and the University of Southampton, United Kingdom. He received the Dipl.-Ing. degree and the Dr.-Ing. degree in electrical engineering from the University of Karlsruhe, Germany, in 2000 and 2005, respectively.

From 2000 to 2005, he was a research assistant in the Communications Group at the University of Karlsruhe. Working on a collaborative project to build a humanoid robot, his research focused on the man-machine interface and in particular the audio-visual attention system as well as audio-visual speaker tracking and identification. In 2005, he joined the Digital Audio Processing Laboratory, Thomson Corporate Research, Hannover, Germany. He is not only engaged in developing advanced audio, but also video processing technologies for production and post-production. His research interests include audio and video processing, data fusion, object tracking, and statistical information theory.

Kristian Kroschel In 1971 he received the Ph.D. degree from the University of Karlsruhe. He studied electrical engineering at the Universities of Karlsruhe and Erlangen-Nürnberg, Germany.

Since 1977 he has been a Professor of Communication Engineering at the Department of Electrical Engineering and Information Technology. From 1987 through 1991 he headed in parallel the group Digital Signal Processing and Diagnosis at the Fraunhofer Institute of Information and Data Processing (IITB) in Karlsruhe. He has held the following positions at the Department of Electrical Engineering and the University of Karlsruhe, respectively: Vice Dean academic year 1982/83, member of the administration board of the university 1984–1992, member of the senate of the university 1986–1990, Student Dean 2000–2002.

On the field of signal processing and communication he has published more than 60 papers and 3 books, partly together with other authors. His special interest is on signal processing of acoustic and video signals applied to man-machine communication. Several times he was a visiting professor, at the Technion Haifa, Israel, the University of California at Santa Barbara, the Bandung Institute of Technology, Indonesia. He is a member of the VDE, the German association of engineers in electrical engineering, electronics, and information technology.